Probe-Beam Deflection Diagnostic of Shock Waves Generated during Direct Laser Interference Patterning

Tobias Steege*[1], Clarita Muntschick[1], Christoph Zwahr[1], and Andrés F. Lasagni[1,2]

[1]*Fraunhofer Institute for Material and Beam Technology IWS, Winterbergstr. 28, 01277 Dresden, Germany*
[2]*Technische Universität Dresden, Institut für Fertigungstechnik, George-Bähr-Str. 3c, 01069, Germany*
**Corresponding author's e-mail: tobias.steege@iws.fraunhofer.de*

Laser-based technologies have become a relevant method for creating microstructured surfaces on materials for enhancing their functionalities. In this field, traditional monitoring methods can be supplemented by analyzing acoustic emissions (AE), offering insights into laser-material interactions for quality control. This study explores the dynamics of laser-induced shock waves and plasma from stainless steel targets under atmospheric conditions using Direct Laser Interference Patterning (DLIP) as well as Direct Laser Writing (DLW). Utilizing optical beam deflection technique, the propagation of a supersonic shock wave and its evolution into an acoustic wave could be measured, alongside the plasma plume. Acoustic emissions from the laser ablation were recorded at various distances, with the explosion blast wave model providing a good estimation of the shock front's temporal development. These emissions originate from the ablation plasma's lifecycle, including expansion, oscillation, and contraction. The performed research enhances the understanding of DLIP and DLW, suggesting new pathways for improved monitoring and control in laser surface patterning.
DOI: 10.2961/jlmn.2025.01.2002

Keywords: direct laser interference patterning, direct laser writing, surface microstructures, acoustic emission, laser-induced plasma monitoring

1. Introduction

Laser technology has revolutionized material processing, particularly in enhancing surface properties through topographical modifications. These advancements enable materials to be integrated into diverse products and applications, ranging from self-cleaning surfaces that repel dirt and dust through hydrophobic properties [1] to surfaces designed for improved adhesion, critical in medical implants for tissue integration [2]. For such surface micro-modifications, techniques such as Direct Laser Writing (DLW) [3], Laser-Induced Periodic Surface Structures (LIPSS) [4], and Direct Laser Interference Patterning (DLIP) [5] have become relevant. In particular, DLIP stands out for its ability to generate periodic micro- and nanoscale structures on surfaces by creating interference patterns with two or more coherent laser beams from a single laser source. By varying the laser's wavelength, polarization, the number of beams, and their intersection angles, a wide range of periodic patterns can be produced. This versatility has led to successful applications for various materials, including metals [6], ceramics [7], and glasses [8].

All laser-based texturing methods usually exhibit low processing tolerances, limited for example to the Rayleigh length for DLW and to the interference volume's vertical extent for DLIP. Such low tolerances require advanced process monitoring solutions to ensure optimal process quality [9,10]. For laser texturing processes as DLW, the analysis of laser beam information such as plasma propagation and acoustic emission has been successfully performed for both monitoring and controlling the process [10,11]. For instance, studies on femtosecond laser interactions with silicon carbide employed acoustic emission (AE) techniques, AE monitoring, combined with high-speed cameras, has been successfully used to study rust removal by pulsed lasers [12]. Contact microphones can also capture surface-acoustic emissions to gather relevant process information, such as variations in pulse energy. Additionally, a correlation between the focal position and the AE could be detected in a previous research [13]. However, results show that surface processing based on AE information remains challenging due to the complex, non-linear ablation process. In addition, it was also shown that the monitoring of the airborne acoustic emission can be similarly used for detecting the focus position for picosecond pulses [13,14]. For established laser processes such as welding and drilling, additional sensors, such as cameras for capturing process lighting/radiation or microphones for recording airborne sound, are commonly used [10].

In case of DLIP, it has been demonstrated that these monitoring processes can be transferred and applied effectively. For example, the ideal working position and the spot diameter on the material could be determined by measurement at different z-positions (acoustic sweep) [15]. Additionally, by applying machine learning algorithms it was shown, that additional information from the process can be read, e.g. as the spatial period of the interface pattern [15]. The above mentioned monitoring approaches, that have been implemented for DLW and DLIP, rely on the emissions of the plasma that is generated during laser ablation. As the laser beam evaporates and ionizes material, a plasma plume is created that expands depending on the laser pulse stability, surrounding atmosphere conditions, and material characteristics. This phenomenon is used for instance in the well-

known solid sampling method for analytical techniques such as Laser Ablation Inductively Coupled Plasma Mass Spectrometry (LA-ICP-MS) [16].

For analyzing laser ablative processes, different approaches can be used, including the measurement of the deflection of a probe beam by the plasma plume with a photodiode, or directly recording the plasma plume with a high speed camera (shadowgraphy). Shadowgraphy is an optical method to observe non-uniformities in transparent media that allows to visualize the high-dynamic effects occurring in micro-material ablation. It this case it has been shown that at higher pulse repetition frequencies, the ablation plume of consecutive pulses overlap, forming a closed cloud [17].

For camera-based time-resolved analysis of the process, the pump and probe laser beams are delayed relative to each other, stitching different laser pulses for the analysis together. This approach relies on two pulsed laser sources, whereby the probe beam has to have a shorter pulse duration than the pump beam. For measuring the deflection of the shockwave, a continuous wave laser can be used. Here, the speed of the shockwave and consequently the shockwave energy can be calculated. For ceramics, it has been shown that for short laser pulses, a relationship between the ablation rate and the shockwave energy can be made, and therefore different regimes of interaction can be detected [18]. All of these monitoring approaches and analysis of the shockwave were done for direct laser ablation where only one source of shockwave is generated. However, none of these methods have been applied to the DLIP technique so far.

In this work, the analysis of the spatio-temporal development of single-pulses irradiation plasma plume is studied, revealing the supersonic shockwave and the plasma plume expansion for DLIP. In particular, it focuses on comparing the shockwave propagation for different spatial periods and comparing the results to the air-borne acoustic emissions of the process.

2. Materials and Methods

2.1 Materials

Flat samples made of X5CrNi18-10 austenitic stainless steel (EN 1.4301 / AISI 304) with a thickness of 0.7 mm and dimension of 55 mm x 40 mm were used for the experiments. The surfaces have a surface roughness Sa of ~ 70 nm (electro-polished; measured according DIN-ISO 25178) and all surfaces were cleaned from contaminations prior to the laser treatment using ethanol.

2.2 Experimental setup

The plasma plume expansions during DLIP ablation on a stainless-steel target was monitored using a pump probe laser beam setup. The probe laser was oriented parallel to the sample surface and crosses through the plasma plume above the DLIP ablation spot. When the plasma plume expands into the path of the pump probe laser beam, it is deflected. This deflection is monitored by a photodiode.

The distance between the surface and the probe-beam axis of propagation was varied for each pulse in the range of 20 µm up to 2 mm to obtain a spatial mapping of local perturbations. Figure 1 shows the experimental setup used for both DLIP and DLW approaches, including the acoustic sensor and the probe-beam deflection setup.

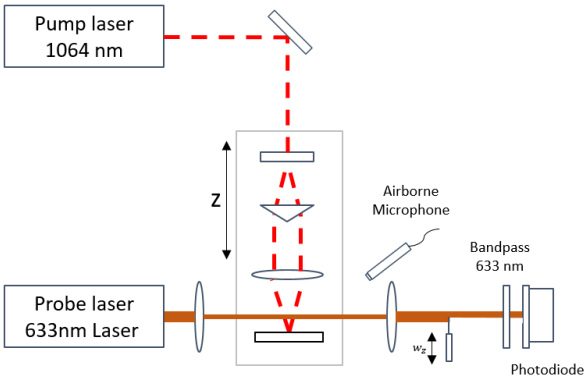

Fig 1 Schematic of the employed experimental setup-up, showing the two beam DLIP configuration, the position of the microphone and the pump-probe beam setup.

For the DLIP experiments, a two-beam configuration was used. In this case a coherent laser beam is divided into two sub-beams by a diffractive optical element (DOE), parallelized by a pyramid, and superimposed by a lens on the sample surface. For the DLW experiments, both the DOE and pyramid were removed, and for both laser approaches an aspheric focusing lens with a focal length of 40 mm was chosen. The used laser source was a Q-switched Nd:YLF laser (Laser export Tech-1053 Basic, Moscow, Russia) with a wavelength of 1053 nm generating 12 ns pulses with pulse energies up to 290 µJ (at 1 kHz). The sample holder, as well as all the optical elements are fixed to an axis, which can be moved independently of the probe-beam.

The probe-beam was provided by a HeNe Laser with a wavelength of 633 nm, which was focused by a lens (f=150 mm) to produce a focal spot of 100 µm waist diameter in the interaction region. Beam deflections induced by a change in the refractive index of the air above the ablation area are measured by masking half the beam on the photodiode with a knife edge. A change in the refractive index results in a deflection of the beam and consecutively a variation in the exposed area of the photodiode (see Figure 1). To reduce the influence of the beam waist, a second lens with a focus lens of -150 mm was set in front of the knife. The photodiode (PDA36A-EC, Thorlabs, USA) with a bandwidth of 5.5 MHz is connected to an oscilloscope (HMO3004, Rohde&Schwarz, Germany). The knife blocks, in stationary conditions, half of the probe beam and therefore provides a base voltage. Any beam deflection results in a power increase or decrease, depending on the air density distribution.

For each experiment, the distance between the probe beam and the sample was increased by 25 µm up to a distance to 200 µm, 250 µm to 500 µm, and finally by 500 µm up to a distance of 2 mm. At each position the response of three different laser pulses was recorded at a sampling rate of 10 MHz for a length of 200 milliseconds. The electronic pulse signal of the pump laser is also recorded and used as trigger for the oscilloscope.

In addition, a free-field microphone M30 (Earthworks Audio, Milford, USA) was positioned diagonally above the laser interaction zone, at various distance from 20 up to 40 mm and an oriented angle of 25°, ensuring both beams were symmetrically oriented to the sensor (see Figure 1). While the precise positioning of the microphone is critical to

ensure optimal audio capture, the distance and angle of the sensor only affect the amplitude of the recorded signal and not the characteristic features or the frequency content of the signal itself [15]. The microphone was connected to a computer using an audio mixing console AG06 (Yamaha, Hamamatsu, Japan). Characterized by an omnidirectional measurement capability, the microphone has a frequency bandwidth spanning from 3 Hz to 30 kHz and a sensitivity of 34 mV/Pa. The continuous audio signal was captured with a frequency of 96 kHz, in line with the maximum frequency of interest [15].

2.3 Shock wave modelling

When a laser beam is absorbed by a metallic material, its surface rapidly reaches very high temperatures (when sufficient energy is used). Then, the material can evaporate very rapidly generating a plasma plume. As a consequence, the air around is compressed and a shock wave is produced. The propagation of this shockwave can be distinguished into three different phases, first, the mass phase, which can be described by the Freiwald-Axford model. As the shockwave can be seen as a plane wave, this model is only valid over the distance of the spot diameter. The second phase, where the shockwave has a higher pressure than the ambient gas, is called the blast wave phase and can be described by the Taylor-Sedov model [19]. Here, a mostly spherical-shaped shock wave is induced, as the further material evaporation, the phase explosion and melt ejection generate an expanding particle cloud. In this case, the following equation can be used for describing the temporal course of the plasma expansion:

$$R_{ST}(t) = S(\gamma)\left(\frac{E_o}{\rho_0}\right)^{\frac{1}{2+\xi}} t^{\frac{2}{2+\xi}}. \quad (1)$$

Here, the distance of the shock wave front from the source (R_{ST}), and depends on then initial energy input E_o and the density of the surrounding gas ρ_0. The thermo-dynamic behavior of the gas is given as the function $S(\gamma)$. The shape of the wave is descripted by ξ: $\xi = 1$ for linear propagation, $\xi = 2$ for cylindrical propagation and $\xi = 3$ for spherical propagation. In case of pulsed laser ablation, the following simplified equation can be used for fitting to performed measurements of the shockwave propagation, according to [19]:

$$R_{ST}(t) = At^C. \quad (2)$$

The fit parameters A and C can be used to fit the data. In addition, the maximum vertical distance of the wave from the surface can be approximated by

$$\left(\frac{3M_o}{2}\right) \ll R_{ST} \ll \left(\frac{E_0}{\rho_0}\right)^{1/3}, \quad (3)$$

where M_o is the initial explosion mass and ρ_0 is the ambient pressure. In this domain the shock wave propagates with supersonic speed in the surrounding medium till the overpressure becomes of the order of the ambient gas pressure (third phase). Thereby it takes on a hemispherical form and slowing down to the speed of sound of the medium v_{sw}. Therefore, the movement of the shockwave front can be described as free propagation

$$R_f(t) = v_{sw}t + n, \quad (4)$$

where the distance R_f is proportional to the time t. Here n is the fitting factor for the formula.

3. Results and discussion

As mentioned before, the temporal evolution of the beam deflection and, consequently, the change in the diode signal indicates the time of flight of the shockwave between the probe beam and the sample surface. Figure 2 shows two examples of the photodiode signal as a result of a pump beam propagating at two different distances from the surface (50 and 500 µm) and interacting with a plasma plume from a DLIP pulse. This was achieved by the simultaneous movement of the sample and the optical DLIP module in relation to the probe beam, to not change the working position of the setup. Additionally, in Figure 2, the trigger signal of the laser is shown. At both distances, a peak can be observed directly after the laser pulse, which corresponds to the shockwave passing through the probe-beam. Interestingly, the recorded peak at a distance of 50 µm has a long decay of 100 µs, while at 500 µm a peak at the same moment in time and a second increase of the signal at 0.12 ms can be observed. This indicates that both the shock wave and the ablation plume can be detected by the deflection of the probe beam.

For distances of the probe beam to the surface of up to 200 µm, the deflection of the shockwave and plasma are very close, and thus it is not possible to differentiate them as two different peaks. As the ablation plume slows down and

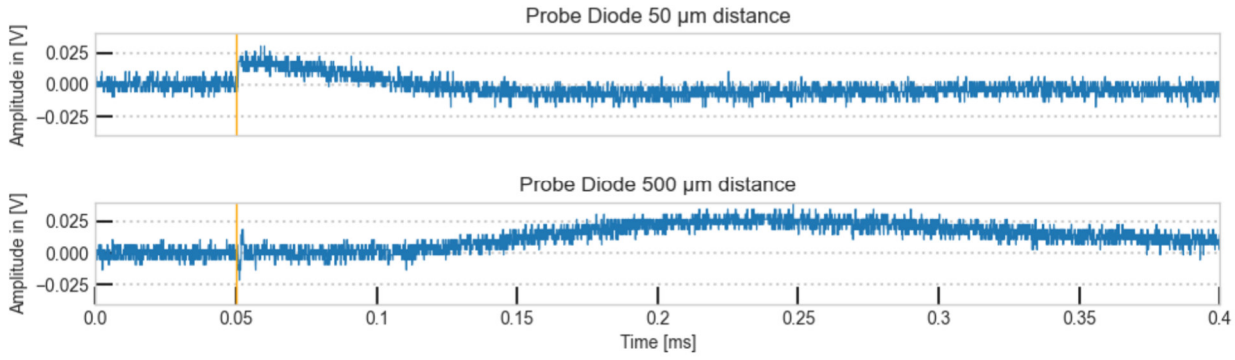

Fig 2 Photodiode signal (blue) and laser trigger signal (orange) at a) 50 µm distance and b) 500 µm between probe beam and sample surface

reaches its maximum height (relative to the material's surface), a longer deflection of the probe beam can be detected.

In a next experiment, the signal of the photodiode at increasing distances between the sample and the probe beam for DLW was captured. For each position, the time between the laser trigger signal and the detection of the first peak through the photodiode was calculated. The position of the peak was determined by an onset detection algorithm [20]. Figure 3 shows the calculated time delay, thus the time of flight of the shock wave for distances between 20 and 2000 µm for single-spot laser ablation for three different laser pulse energies (130 µJ, 170 µJ and 210 µJ).

As can be seen by the overlapping of the curves, no significant increase in the propagation speed of the shockwave for different pulse energies was detected. It can be assumed that energy interval E_o (see Equation 2) does not increase with higher laser power, implying that not all laser energy is used to ablate the material. Instead, a portion of the laser energy is likely absorbed by other processes such as heating the surrounding air, generating plasma, and causing thermal diffusion within the material [18]. In addition, the generated plasma extends along the direction of the probe beam for higher laser energy. Therefore, the propagation of the shockwave could also be influenced by plasma shielding [17].

An approximation of the shockwave in the blast wave phase, fitted as given by Equation 2 and the speed of sound (Equation 4), is shown for DLW pulse energy of 210 µJ (Figure 3). When fitting the data for the whole time interval using Sedov-Taylor model (Equation 2), the equation cannot appropriately describe the measured data. However, when fitting the data for 20 µm up to 200 µm, a good agreement was found with an $R^2 = 0.93$. The latter range of the measured data from 200 µm up to 2000 µm can be fitted by the free propagation model (Equation 3). The calculated parameter for v_{sw} corresponds to the speed of sound of 343 m/s. As it can be observed, the propagation of the shockwave for DLW is equivalent to the values given in the literature and the shock wave is supersonic in the range up to 500 µm and transforms to an acoustic wave, travelling at the speed of sound [21].

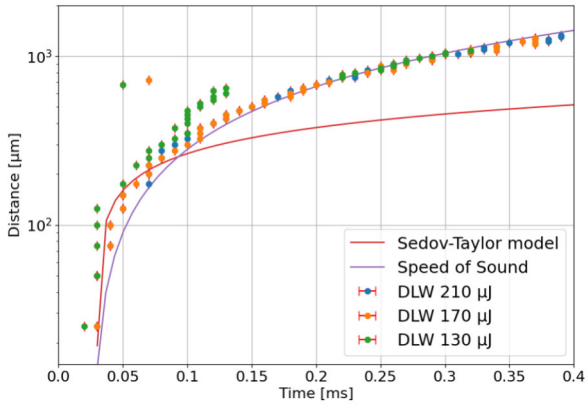

Fig 3 Propagation of a shock wave generated by the pulse ablation process for different laser pulse energies and the fit of the shock wave modeling.

After that, the shockwave propagation for DLIP was recorded, therefore the experiments were repeated for different interference periods. Figure 4 shows the time of flight of a shockwave generated by DLIP for different spatial periods (6 µm, 8 µm and 10 µm) for 215 µJ pulse energy. As observed, no difference in propagation speed was observed between the different spatial periods. This indicates that the shockwave generated for DLIP has the same propagation speed and energy in the supersonic domain as for direct ablation using DLW. Additionally, only one peak in the photodiode signal (see Figure 2) was observed, indicating a single shockwave.

Given the expansion rate of the shockwave and the distance of the probe beam to the sample surface, it can be assumed that only one ablation event is generated in the DLIP-laser spot. As can be observed by the fit of the speed of sound, the shockwave slows down similarly as the DLW shockwave as indicated in Figure 3. In addition, the ablation plume rising time is shown as the time difference between the laser pulse and ablation peak in the signal (blue data-points). As can be seen, from 200 µm upwards, a distinction between those to signals can be made.

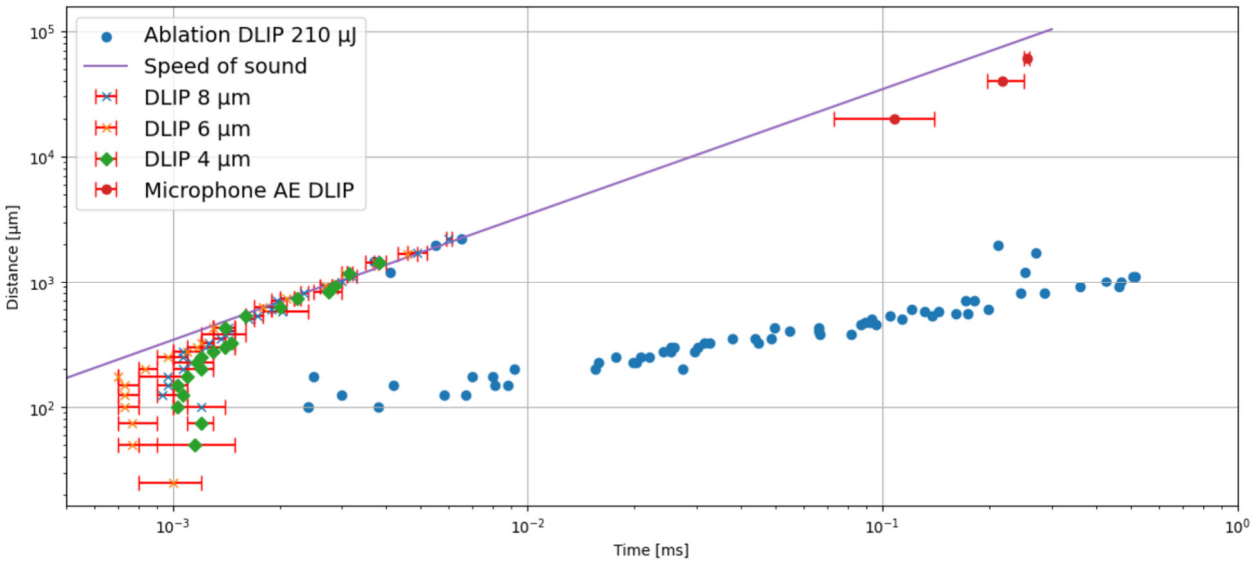

Fig 4 Propagation of the shockwave generated by Direct laser interference patterning for different spatial periods, propagation of a secondary acoustic wave by and the propagation of the plasma plume.

In addition, the acoustic emissions originating from the ablation events were measured by a microphone for the above described experiments. The measurement of the arrival time of the AE captured by the microphone at a position of 2 cm, 3 cm and 4 cm from the ablation for 210 µJ are shown in Figure 4 (red data-points). As can be seen, this signal arrival times are below the extended fit for the speed of sound. This indicates that the acoustic wave measured by the airborne microphone is not identical to the shockwave generated by the laser ablation. This could indicate a two-stage wave generation process for surface texturing: first, a shockwave due to the rapid expansion caused by the initial impact of the laser pulse on the material, and second, an acoustic wave generated by the dynamics of the plasma. The acoustic wave generation results from the dynamics of the plasma (expansion, oscillation, and contraction) [22].

These waves could have lower initial energy compared to the initial shockwave and therefore would directly propagate at the speed of sound. Such a low-energy wave could be the sound typically associated with the laser-plasma interaction but, due to the lower energy, this wave cannot be captured with the probe-beam approach. Additionally, during the first stage of the plasma plume, the distinction between these two phases might not always be clear, as they occur in rapid succession and might overlap depending on the conditions of the laser-material interaction. This observation suggests that while the Sedov-Taylor model effectively describes initial shock wave propagation, the complete plasma dynamics may require additional theoretical considerations to account for extended energy release profiles [23]. The identification of a two-stage wave generation process, consisting of an initial shock wave followed by an acoustic wave from plasma dynamics, suggests that no direct connection between the airborne acoustic signal and the interference pattern can be made. However, this also implies that a correlation between the acoustic signal and the ablated material should be possible.

4. Conclusion

In this work, the dynamics of shock waves and plasma behavior during Direct Laser Interference Patterning (DLIP) and Direct Laser Writing (DLW) on stainless steel were investigated. The first objective was to analyze the shockwave propagation during laser ablation.

For the time-resolved analysis of the ablation process, a pump probe laser beam setup was used, where the distance between of the probe beam to the ablation on the surface was increased up to 2 mm, and the deflection of the probe beam was measured by a photodiode. In single pulse ablation experiments, the propagation speed of the shockwave was determined as supersonic below 500 µm and slowing down to the speed of sound. In addition, it was also found that the experimentally determined shockwave propagation speed for both the supersonic and speed of sound regimes is in good agreement with theoretical models. This indicates that typical acoustic process monitoring approaches that are used for DLW can also be applied to DLIP. By comparing the results of the acoustic measurements taken by airborne microphones, it was indicated that two acoustic waves may be generated by the ablation process, consisting of an initial shock wave followed by an acoustic wave created by the plasma.

Future research will focus on isolating and characterizing plasma-induced acoustic waves separately from initial shock waves. Advanced diagnostics, such as high-speed imaging and spectroscopy, combined with machine learning algorithms, could improve the precision and predictive capabilities of these monitoring systems.

Acknowledgments

This work was funded partially by the European Union under grant agreement no. 101091514 and the German Federal Ministry of Education and Research (BMBF) within the framework concept “Zukunft der Wertschöpfung – Forschung zu Produktion, Dienstleistung und Arbeit“ (funding code 02P20A050 – 02P20A057). The work of A.L. was supported by the German Research Foundation (DFG), Excellence Initiative by the German federal and state governments to promote top-level research at German universities (Grant no. F-003661-553-41A-1132104).

References

[1] S. Milles, M. Soldera, T. Kuntze, and A. F. Lasagni: Appl. Surf. Sci., 525, (2020) 146518.
[2] A. Hariharan, P. Goldberg, F. Schell, U. Hempel, F. Striggow, M. Hantusch, M. Medina-Sánchez, A. F. Lasagni, and A. Gebert: Adv. Funct. Mater., 34, (2024) 2310607.
[3] I. Etsion: J. Tribol.-Trans. Asme, 127, (2005) 248.
[4] S. Alamri, F. Fraggelakis, T. Kunze, B. Krupop, G. Mincuzzi, R. Kling, and A. F. Lasagni: Materials, 12, (2019) 1018.
[5] A. Madelung, S. Alamri, T. Steege, B. Krupop, A. F. Lasagni, and T. Kunze: Adv. Eng. Mater., (2021) 2001414.
[6] M. Bieda, A. F. Lasagni, and E. Beyer: Proc. International Congress on Applications of Lasers & Electro-Optics, (2010) 900.
[7] D. Fabris, A. F. Lasagni, M. C. Fredel, and B. Henriques: Ceramics, 2, (2019) 578.
[8] S. Alamri, P. A. Sürmann, A. F. Lasagni, and T. Kunze: Adv. Opt. Technol., 9, (2020) 79.
[9] M. Chaja, T. Kramer, and B. Neuenschwander: Procedia CIRP, 74, (2018) 300.
[10] T. Purtonen, A. Kalliosaari, and A. Salminen: Phys. Procedia, 56, (2014) 1218.
[11] J. Luo, Y. Liang, and G. Yang: Rev. Sci. Instrum., 83, (2012) 053102.
[12] X. Xie, Y. Zhang, Q. Huang, Y. Huang, W. Zhang, J. Zhang, and J. Long: J. Mater. Process. Technol., 290, (2021) 116990.
[13] E. V. Bordatchev and S. K. Nikumb: Meas. Sci. Technol., 13, (2002) 836.
[14] E. V. Bordatchev and S. K. Nikumb: Appl. Surf. Sci., 253, (2006) 1122.
[15] T. Steege, S. Alamri, A. F. Lasagni, and T. Kunze: Sci. Rep., 11, (2021) 14540.
[16] P. N. Soltanpour, G. W. Johnson, S. M. Workman, J. B. Jones, and R. O. Miller,Society of Agronomy, (2018) 91.
[17] S. Kraft, J. Schille, S. Mauersberger, L. Schneider, and U. Loeschner: Proc. Laser-based Micro- and Nanoprocessing XIV, (2020) 11268.

[18] K. Alnama, N. Sulaiman, and I. Ibrahim: Optik, 246, (2021), 167832.
[19] J. S. Díaz and S. E. Rigby: Shock Waves, 32, (2022) 405.
[20] F. Bai, D. Gagar, P. Foote, and Y. Zhao: Mech. Syst. Signal Process., 84, (2017) 717.
[21] C. Stauter, P. Gérard, J. Fontaine, and T. Engel: Appl. Surf. Sci., 109–110, (1997) 174.
[22] N. Hosoya, I. Kajiwara, T. Inoue, and K. Umenai: J. Sound Vib., 333, (2014) 4254.
[23] X. Mao, S. Wen, and R. E. Russo: Appl. Surf. Sci., 253, (2007) 6316.

(Received: July 25, 2024, Accepted: December 29, 2024)